



Research Paper

Pt supported on ordered microporous carbon as highly active catalyst for catalytic hydrodeiodination of iodinated X-ray contrast media



Hui Liu^a, Qing Yu^a, Heyun Fu^a, Yuqiu Wan^a, Xiaolei Qu^a, Zhaoyi Xu^{a,*}, Daqiang Yin^b, Shourong Zheng^{a,*}

^a State Key Laboratory of Pollution Control and Resource Reuse, Jiangsu Key Laboratory of Vehicle Emissions Control, School of the Environment, Nanjing University, Nanjing 210093, PR China

^b Key Laboratory of Yangtze River Water Environment of Ministry of Education, Tongji University, Shanghai 200092, PR China

ARTICLE INFO

Keywords:

Supported Pt catalysts
Zeolite templated carbon
Pt exchanged Y zeolite
Liquid phase catalytic hydrodeiodination
Iodinated X-ray contrast media

ABSTRACT

In this study, Pt catalysts supported on zeolite templated carbon (Pt/ZTC) were prepared by *in-situ* chemical vapor deposition using Pt exchanged Y zeolite as the template. For comparison, Pt catalysts supported on zeolite templated carbon (ZTC) and commercial activated carbon (AC) were prepared using the impregnation method. The liquid phase catalytic hydrodeiodination of two iodinated X-ray contrast media (ICM, *i.e.*, diatrizoate and iopamidol) was investigated on the catalysts. The catalysts were characterized by X-ray diffraction, N₂ adsorption–desorption isotherms, scanning electron microscope, transmission electron microscopy, X-ray photoelectron spectroscopy and zeta-potential measurement. The results showed that Pt/ZTC catalysts prepared by *in-situ* chemical vapor deposition (CVD) under varied reaction conditions were good replicas of Y zeolite in structure. Compared with the catalysts prepared by the impregnation method, Pt/ZTC had a higher Pt dispersion and more homogeneous Pt distribution. Increasing CVD temperature resulted in Pt particle growth in Pt/ZTC. The catalytic hydrodeiodination of diatrizoate and iopamidol proceeded via a sequential deiodination pathway, and followed the Langmuir–Hinshelwood model, reflecting that the conversion of adsorbed ICM was the rate-controlling step. Additionally, more effective conversion of iopamidol was observed than that of diatrizoate on Pt/ZTC. Furthermore, Pt/ZTC prepared at higher CVD temperature exhibited lower catalytic activities for the hydrodeiodination of diatrizoate and iopamidol. Solution pH markedly impacted the catalytic ICM conversion, and enhanced hydrodeiodination was observed with the increase of pH. As for catalyst reuse, Pt/ZTC remained about 80% of initial activity after 4 reuse cycles, exhibiting much higher stability than the catalyst prepared by the impregnation method. The present findings highlighted the Pt/ZTC catalysts prepared by *in-situ* CVD as highly active and stable catalysts for the removal of halogenated organic pollutants by catalytic hydrogenation.

1. Introduction

Iodinated X-ray contrast media (ICM) have been widely used to enhance the imagination of the soft tissues (*e.g.*, organs, veins, and blood vessels) for clinical diagnosis [1]. ICMs are designed to be chemically inert and to be excreted into the urine in unmetabolized forms within 24 h [2]. As a result, these chemicals were highly stable in natural aquatic environment and very refractory against most biological and chemical wastewater treatment processes because of their high biochemical stability and hydrophilic properties [3,4]. Accordingly, ICMs have been frequently detected in the aquatic environment with elevated concentration levels [5,6]. Previous research concluded that ICM contributed to more than 90% of the organic iodine in wastewater and surface water [7]. Duirk et al. [8] reported that ICM

transformation induced the formation of iodinated disinfection by-products, such as iodo-acids and iodo-trihalomethanes, which were highly cytotoxic and genotoxic. Therefore, it is very urgent to develop reliable methods to eliminate the pollution from ICM in aquatic environments.

Intensive research has been conducted to eliminate ICM pollution in environment, such as sorption [9,10], advanced oxidation processes [11,12] and reduction methods [13,14]. Recently, liquid phase catalytic hydrogenation has attracted extensive industrial and academic interest as a simple, safe and effective technique which can be operated under gentle reaction conditions and wide concentration range of target pollutants [15–17].

Supported noble metals (*e.g.*, Pd, Pt, Rh or Ru) [17–20], have been considered as effective catalysts for the liquid phase catalytic

* Corresponding authors.

E-mail addresses: zhaoyixu@nju.edu.cn (Z. Xu), srzhseng@nju.edu.cn (S. Zheng).

hydrodehalogenation, and metal oxides and carbonaceous materials were usually used as catalyst supports. In comparison with metal oxides, carbonaceous materials were commonly adopted due to their high stability towards acidic and basic reaction conditions [21]. However, noble metal catalysts supported on carbonaceous material prepared by conventional methods (e.g., impregnation method) normally had large metal particles, and were susceptible to metal loss and irreversible catalyst deactivation due to weak metal-support interaction [22,23]. Confining active metals in porous supports provided an effective way to prepare highly dispersed and stable catalysts [24]. For example, Shao et al. [25] studied the catalytic hydrodechlorination of chlorophenol and observed much higher and more stable catalytic activity of Pd supported on mesoporous carbon than that on activated carbon. In parallel, similar results were observed in other liquid phase catalytic hydrogenation reactions [26,27].

Pt particles confined in ordered microporous carbon synthesized via zeolite templating method have been studied for hydrogen storage and electrical catalysis. Through chemical vapor deposition (CVD) and carbonization at high temperature (e.g., 900 °C), a porous carbon material with well-defined Pt clusters and narrow size distribution could be obtained due to effective confinement effects [28,29]. Despite of their remarkable advantages, the materials have been seldom used as catalysts in liquid or gas phase catalysis. We hypothesized that metallic Pt particles supported on zeolite templated microporous carbon prepared by the *in-situ* CVD method may exhibit substantial advantages for the catalytic hydrodehalogenation. However, studies on liquid phase catalytic hydrodehalogenation on the catalysts have not been conducted thus far.

In this study, we synthesized a series of Pt catalysts supported on ordered microporous carbon prepared using Pt exchanged zeolite Y as the template for the liquid phase catalytic hydrodeiodination of two typical ICM (i.e., diatrizoate (DTZ) and iopamidol (IOP)). For comparison, Pt catalysts supported on activated carbon and zeolite-templated carbon (ZTC) were prepared by the traditional impregnation method. The catalysts were characterized and the mechanism of catalytic hydrodeiodination of DTZ and IOP on the catalysts was systematically investigated.

2. Experimental

2.1. Chemicals and materials

DTZ and IOP were purchased from Aladdin and Jiaxing Si Cheng Chemical Co., Ltd (China), respectively. $\text{Pt}(\text{NH}_3)_4(\text{NO}_3)_2$ was purchased from Sigma-Aldrich. Na-Y zeolite with $\text{SiO}_2/\text{Al}_2\text{O}_3$ ratio of 5.5 was obtained from Catalyst Plant of Nankai University, China. A bituminous coal derived activated carbon (Filtrasorb-300, AC) was purchased from Calgon Carbon Co., USA and was used as received. All chemical reagents were of analytical grade and used as received without further purification.

2.2. Catalyst preparation

The template Pt exchanged Y zeolite with a Pt loadings of 1 wt.% was first prepared using the ion exchange method [30,31]. Briefly, 2 g of Na-Y zeolite was suspended in 1000 ml distilled water containing 2 ml of $0.01 \text{ g l}^{-1} \text{ Pt}(\text{NH}_3)_4(\text{NO}_3)_2$. The ion exchange was carried out at 80 °C for 10 h under stirring. Pt-exchanged Y zeolite was collected by filtration, followed by washing with deionized water to remove excess Pt salt, and drying at 60 °C overnight. The resultant Pt exchanged zeolite was heated to 350 °C in a muffle furnace with a ramping rate of 0.5 °C min⁻¹, and calcined at 350 °C in air for 2 h. Then, the Pt-zeolite template was reduced under a H_2 stream (40 ml min⁻¹) at 320 °C for 2 h.

The Pt catalysts supported on ZTC were prepared using the *in-situ* CVD method [32,33]. To obtain high yield and suppress Pt aggregation,

furfuryl alcohol (FA) was first filled in zeolite pores. Briefly, 1.5 g of Pt exchanged zeolite was loaded in a glass filter bottle equipped with a sealing plug, which was degassed at room temperature for 1 h. Furfuryl alcohol was added in the bottle, which was stirred at room temperature for 24 h under reduced pressure. The mixture was filtrated and washed with mesitylene to remove excess FA from zeolite external surface. The Pt-zeolite/FA composite was then heated at 80 °C for 24 h under a flow of N_2 (100 ml min⁻¹), followed by heating at 150 °C for another 8 h. The resultant composite was loaded in a tubular furnace, which was further pyrolyzed under propylene gas (4.0% in N_2) with a flow rate of 100 ml min⁻¹ for 3 h. The pyrolyzation temperature varied from 700 to 800 °C. Then, the sample was subjected to thermal treatment at 900 °C under N_2 flow for another 3 h. After cooling to room temperature, the zeolite template in the carbon/zeolite composite was removed by stirring in 27 M hydrofluoric acid (HF) at 20 °C for 4 h. X-ray photoelectron spectroscopy analysis showed that the residual Si and Al contents were below the detectable level. Pt catalyst supported on ZTC was obtained after washing by deionized water and drying at 80 °C overnight. The resultant catalysts were designated as Pt(X)/ZTC-Y, where X is Pt loading (wt.%) determined by inductive coupled plasma emission spectrometer, and Y is CVD temperature (°C). To prepare ZTC supported Pt catalysts by the impregnation method, ZTC support was prepared by the same method but using Na-Y zeolite as the template instead of Pt exchanged Y zeolite, and CVD was conducted at 700 °C.

For comparison purpose, Pt catalysts supported on ZTC and commercial AC F300 were also prepared using the impregnation method. Briefly, 0.5 g of ZTC or AC was impregnated with 1.5 ml of $0.01 \text{ g l}^{-1} \text{ Pt}(\text{NH}_3)_4(\text{NO}_3)_2$ solution under stirring for 2 h, followed by drying at 80 °C for 12 h, calcining at 350 °C in N_2 for 4 h, and then reducing at 320 °C in a H_2 stream (40 ml min⁻¹) for 2 h. The resultant catalysts were denoted as *im*-Pt(X)/ZTC and *im*-Pt(X)/AC, where X is Pt loading.

2.3. Catalyst characterization

The Pt contents of catalysts were measured by inductive coupled plasma emission spectrometer (ICP) (J-A1100, Jarrell-Ash, USA). The structures of catalysts were determined in the range of 2θ from 5° to 80° by X-ray diffraction (XRD) using Rigaku D/max-RA powder diffractometer (Rigaku, Japan) with $\text{Cu K}\alpha$ radiation at 40 kV and 150 mA with a scanning speed of 2 min⁻¹. Nitrogen adsorption/desorption isotherms and pore size distributions of the catalysts were obtained on a Micrometrics ASAP 2020 (Micromeritics Instrument Co., USA) apparatus at -196 °C (77 K). The samples were outgassed under vacuum at 300 °C for 3 h prior to the nitrogen adsorption measurements. Transmission electron microscopy (TEM) images of the catalysts were recorded on a JEM-2100 transmission electron microscope (JEM-2100, JEOL, Japan) at an accelerating voltage of 200 kV. The valence states of the elements were analyzed by X-ray photoelectron spectroscopy (XPS) analysis using a PHI5000 VersaProbe equipped with a monochromatized $\text{Al K}\alpha$ excitation source ($h\nu = 1486.6$ eV) (ULVAC-PHI, Japan). The C 1 s peak (284.6 eV) was used for the calibration of binding energy. The morphologies of the samples were observed on a Hitachi S-3400N scanning electron microscope. Surface zeta potentials of samples were measured using a Zeta Potential Analyzer (Zeta PALS, Brookhaven Instruments Co.). Prior to zeta-potential measurement, the samples were dispersed in deionized water with a dosage of 0.1 g l^{-1} . The solution pH was adjusted by 0.1 M HCl or 0.1 M NaOH, and the suspension was equilibrated for 24 h before measurement.

2.4. Liquid phase catalytic hydrodeiodination of DTZ and IOP

The catalytic hydrogenation reactions were performed at room temperature and atmospheric pressure in a 250 ml of four-necked flask with a sample port, H_2/N_2 inlet and outlet. Solution pH was kept at 7.0 using phosphate buffer solution. Preliminary experiments showed that prior to catalytic reaction adsorption reached equilibrium within

30 min and the removal of ICMs due to catalyst adsorption was below 3% under our experimental conditions. Briefly, 15 mg of catalyst was added in a flask containing 200 ml of 0.5 mM ICM solution and 200 ml of buffer solution. The reactor was magnetically stirred and purged continuously with a N_2 flow (100 ml min^{-1}) for 40 min to reach adsorption equilibrium. Then, the reaction was started by switching the N_2 flow into a H_2 flow (250 ml min^{-1}). Samples were taken at selected time intervals. The catalyst powder was filtrated using a $0.45 \mu\text{m}$ filter membrane and the residual concentrations of DTZ or IOP, potential intermediates and final products in the filtrates were determined by a high performance liquid chromatography (Agilent 1200 Series HPLC system) with an ultraviolet detector at 238 nm. A reversed phase C18 column ($150 \times 4.6 \text{ mm}$, $5 \mu\text{m}$, Agilent) with 10 mm guard column was used as the stationary phase and the temperature of the column remained at 20°C . The mobile phase consisted of methanol (mobile phase A) and 25 mM sodium dihydrogen phosphate (mobile phase B, a buffer solution with pH of 3). The final pH of the mobile phase was adjusted using orthophosphoric acid. For the analysis of DTZ, the elution rate of the column was 0.8 ml min^{-1} using an elution program of 12% A and 88% B for 6 min, changing to 22% A and 78% B within 9 min, and holding for 18 min, followed by decreasing linearly back to 12% A and 88% B within 20 min and holding for additional 3 min to re-equilibrate the column. As for the analysis of IOP, the rate of elution was 0.6 ml min^{-1} , and the elution program consisted of 4% A and 96% B for 10 min, increasing linearly to 12% A and 88% B within 2 min, and maintaining for 16 min, followed by decreasing linearly back to 4% A and 96% B within 18 min and holding for additional 3 min to re-equilibrate the column.

The possible intermediates and products from catalytic hydrodeiodination of DTZ and IOP were determined on an Agilent 1260 ultra-performance liquid chromatography equipped with a high-resolution hybrid quadrupole time-of-flight mass spectrometry (LC-MS-Triple TOF 5600, AB Sciex, Foster City, CA) hyphenated to an electro-spray interface (ESI) source. The samples were separated using an ACQUITYTM U-HPLC BEH C18 column ($2.1 \text{ mm} \times 50 \text{ mm}$; $1.7 \mu\text{m}$) (Waters, Milford, MA, USA) at 30°C . The isocratic mobile phase consisted of 10% methanol (0.1% formic acid, v/v) and 90% water (0.1% formic acid, v/v) with a flow rate of $200 \mu\text{l min}^{-1}$. The injection volume was $5 \mu\text{l}$ and elution time was 20 min for DTZ and 8 min for IOP. Mass spectrometric analysis was conducted with a TOF-MS operating in a positive ion mode with an electrospray ion source. Mass range was set at m/z 80–1000.

3. Results and discussion

3.1. Catalyst characterization

The XRD patterns of Na-Y, ZTC and supported Pt catalysts are shown in Fig. 1. Very strong diffraction peaks were observed on Na-Y zeolite, and the most intensive diffraction peak with 2θ at 6° was characteristic of the (111) plane of Na-Y zeolite. For ZTC, a strong diffraction peak was identified with 2θ at 6° , reflecting the periodic ordered arrangement of micropores replicated from zeolite Y template [34]. For supported Pt catalysts, three small but clear diffraction peaks were observed at 40° , 46° and 67° , respectively, assigned to (110), (200) and (220) planes from metallic Pt with face centered cubic (fcc) crystallographic structure [30], confirming the successful loading of Pt particles on ZTC. Notably, the structural ordering of ZTC in the supported catalysts differed with preparation conditions, as reflected by the variation of intensity of characteristic peak at 6° with CVD temperature. For example, increasing CVD temperature during the carbonization process resulted in decreased intensity of the characteristic peaks at 6° , reflecting the formation of ZTC with low structural ordering. The lower ordering of ZTC with CVD at 800°C was likely due to structural collapse of Y zeolite [33]. Additionally, the broad peaks around 20 – 30° characteristic of amorphous carbon presented, and their intensities increased with CVD temperature, reflecting enhanced

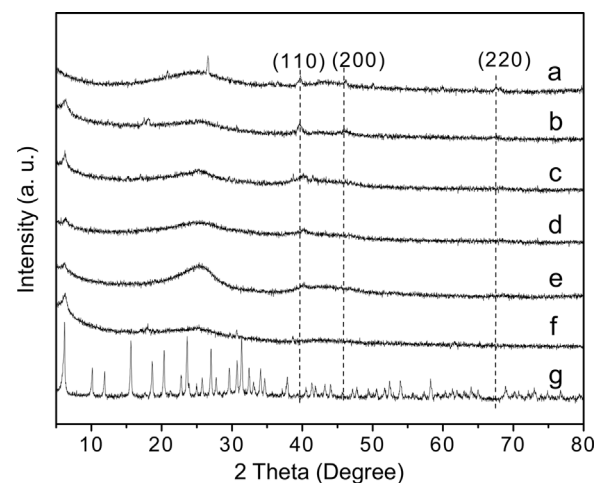


Fig. 1. XRD patterns of (a) *im*-Pt(2.6)/AC; (b) *im*-Pt(2.7)/ZTC; (c) Pt(2.5)/ZTC-700; (d) Pt(2.1)/ZTC-750; (e) Pt(1.4)/ZTC-800; (f) ZTC; (g) Na-Y.

carbonization process occurring on external surface of Y zeolite. As a result, the proportions of the graphitic carbon were high [29].

The morphologies of the supported Pt catalysts were observed using SEM (results presented in Fig. S1, Supporting information). Similar to its template Y zeolite, SEM images of ZTC displayed typical crystalline morphologies with very smooth surface, reflecting a good replica from Y zeolite. For supported Pt catalysts prepared at a high CVD temperature, rough external surface was observed (see Pt(2.1)/ZTC-800 in Fig. S1), confirming carbon deposition on external surface of zeolite template [35].

The N_2 adsorption-desorption isotherms and pore size distributions of the supported Pt catalysts are compiled in Figs. 2 and S2, respectively, and the resultant structural parameters are compared in Table 1. In comparison with *im*-Pt(2.6)/AC, Pt catalysts supported on ZTC had higher specific surface areas and pore volumes, while for Pt catalysts supported on ZTC much lower specific surface area and pore volume were observed on Pt(1.4)/ZTC-800, again suggesting the structural collapse of Y zeolite during treatment at high CVD temperature [36]. Additionally, micropores with pore size around 1.5 nm dominated in Pt catalysts supported on ZTC, reflecting the microporous nature of the catalysts.

Fig. 3 presents the TEM images and histograms of Pt particles of supported Pt catalysts. For *im*-Pt(2.7)/ZTC, Pt particles were not homogeneously distributed, and aggregated Pt particles were clearly identified on ZTC. Considering the ordered pore structure of ZTC, homogeneous Pt distribution could be obtained if Pt particles were loaded into ZTC pores. However, the presence of unevenly distributed and aggregated Pt particles suggested a higher concentration of Pt particles on the external surface of ZTC than for Pt(2.5)/ZTC-700. On

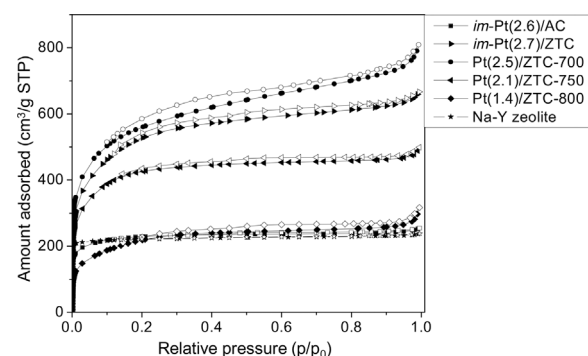


Fig. 2. N_2 adsorption-desorption isotherm of Pt-based catalysts. Filled symbols denote adsorption data and open symbols denote desorption data.

Table 1
Pore structure parameters of Pt-based catalysts.

	S_{BET}^a $\text{m}^2 \text{g}^{-1}$	V_{mic}^b $\text{cm}^3 \text{g}^{-1}$	V_t^c $\text{cm}^3 \text{g}^{-1}$
Na-Y zeolite	704	0.31	0.36
<i>im</i> -Pt(2.6)/AC	662	0.26	0.38
<i>im</i> -Pt(2.7)/ZTC	1630	0.23	0.99
Pt(2.5)/ZTC-700	1731	0.38	1.18
Pt(2.1)/ZTC-750	1332	0.33	0.73
Pt(1.4)/ZTC-800	691	0.05	0.43

^a Determined by N_2 adsorption using the Brunauer–Emmett–Teller (BET) method.

^b Micropore volume, calculated using the Horvath–Kawazoe method.

^c Total pore volume, determined at $P/P_0 = 0.98$.

the contrary, very even distribution of Pt particles was observed on Pt(2.5)/ZTC-700, Pt(2.1)/ZTC-750 and Pt(1.4)/ZTC-800 (See Fig. 3). Additionally, increasing CVD temperature led to a shift of Pt particle distribution to large size, reflecting gradual growth of Pt particles. The average Pt particle sizes in the catalysts were further estimated based on surface area weighted diameter:

$$\bar{d}_s = \sum n_i d_i^3 / \sum n_i d_i^2 \quad (1)$$

where n_i is the counting number of Pt particles with diameter of d_i , and the total counting number (Σn_i) larger than 200.

For catalysts with identical Pt loadings, very broad distributions of Pt particles were observed on *im*-Pt(2.6)/AC and *im*-Pt(2.7)/ZTC, whilst narrow distribution was identified on Pt(2.5)/ZTC-700. The average Pt particle sizes were calculated to be 4.01, 2.98, and 2.32 nm for *im*-Pt(2.6)/AC, *im*-Pt(2.7)/ZTC and Pt(2.5)/ZTC-700, respectively, indicating that *in-situ* CVD resulted in more homogeneous Pt particle distribution and smaller Pt particles as compared to the impregnation method due to effective confinement and embedment effects. Furthermore, CVD temperature may markedly impact catalyst structural properties. For example, Pt particles of Pt(2.5)/ZTC-700 ranged within 1–5 nm, while broad distributions within 1–7 nm were observed on Pt(2.1)/ZTC-750 and Pt(1.4)/ZTC-800. Additionally, the average Pt particle sizes were 2.32, 2.48 and 3.02 nm for Pt(2.5)/ZTC-700, Pt(2.1)/ZTC-750 and Pt(1.4)/ZTC-800, respectively, confirming Pt particle growth with CVD temperature (Table 2).

The XPS analysis was conducted to investigate the chemical properties of Pt particles, and XPS spectra of the reduced catalysts in the Pt 4f region are presented in Fig. S3. The XPS profiles of the catalysts displayed doublet peaks, corresponding to Pt 4f_{5/2} and Pt 4f_{7/2} from spin orbital splitting [37]. Notably, the spectra of the catalysts varied in peak intensity and width, implying the presence of multiple Pt species in the samples. Hence, the XPS spectra of catalysts in the Pt 4f region

Table 2
Properties of supported Pt catalysts.

	Pt content ^a	Pt particle size ^b	Pt dispersion ^c
	(wt.%)	(nm)	(%)
<i>im</i> -Pt(2.6)/AC	2.6	4.01	39.0
<i>im</i> -Pt(2.7)/ZTC	2.7	2.98	52.4
Pt(2.5)/ZTC-700	2.5	2.32	67.3
Pt(2.1)/ZTC-750	2.1	2.48	63.0
Pt(1.4)/ZTC-800	1.4	3.02	51.7

^a Determined by ICP.

^b Calculated from TEM.

^c Calculated from TEM.

were deconvoluted and the results are compiled in Table 3. The spectra could be deconvoluted into two pairs of doublets with the binding energies of Pt 4f_{7/2} of 71.5 and 73.4 eV, assigned to metallic (Pt⁰) and electron-deficient Pt (Ptⁿ⁺), respectively [38]. The presence of Ptⁿ⁺ normally resulted from electron transfer from Pt to support due to the strong metal-support interaction [39]. The contents of Ptⁿ⁺ were calculated to be 28% and 37% on *im*-Pt(2.7)/ZTC and Pt(2.5)/ZTC-700, respectively, indicative of a stronger metal-support interaction in the catalyst prepared by *in-situ* CVD. As for the catalysts prepared by *in-situ* CVD, increasing CVD temperature resulted in lower Ptⁿ⁺/Pt⁰ ratio, likely due to removal of O-containing functionalities at high CVD treatment, thus suppressing the formation of Ptⁿ⁺ [40]. Notably, Pt atomic concentration of Pt(2.5)/ZTC-700 was 0.07, lower than that of *im*-Pt(2.7)/ZTC and *im*-Pt(2.6)/AC, suggesting that Pt particles are predominantly located in the pores of ZTC or embedded beneath ZTC particles. Accordingly, the Pt atomic concentration of *im*-Pt(2.6)/AC was 0.29, much higher than those of other catalysts, reflecting that the majority of Pt particles were located on the external surface.

3.2. Liquid phase catalytic hydrodeiodination of ICM

The hydrodeiodination of DTZ on Pt(2.5)/ZTC-700 with varied catalysts dosages was performed to check if mass transfer limitations existed in the reaction systems, and the results are presented in Fig. S5. The initial reaction rates increased from 0.014 to 0.029 mM min⁻¹ with the increase of catalyst dosage from 0.05 to 0.1 g l⁻¹. After normalization of the reaction rate by catalyst dosage, the reaction rates remained approximately constant, indicating that mass transfer limitations were not present under our experimental conditions.

Because both DTZ and IOP were tri-iodinated compounds, catalytic hydrodeiodination of DTZ and IOP could result in partially and completely deiodinated intermediates and/or products. To illustrate

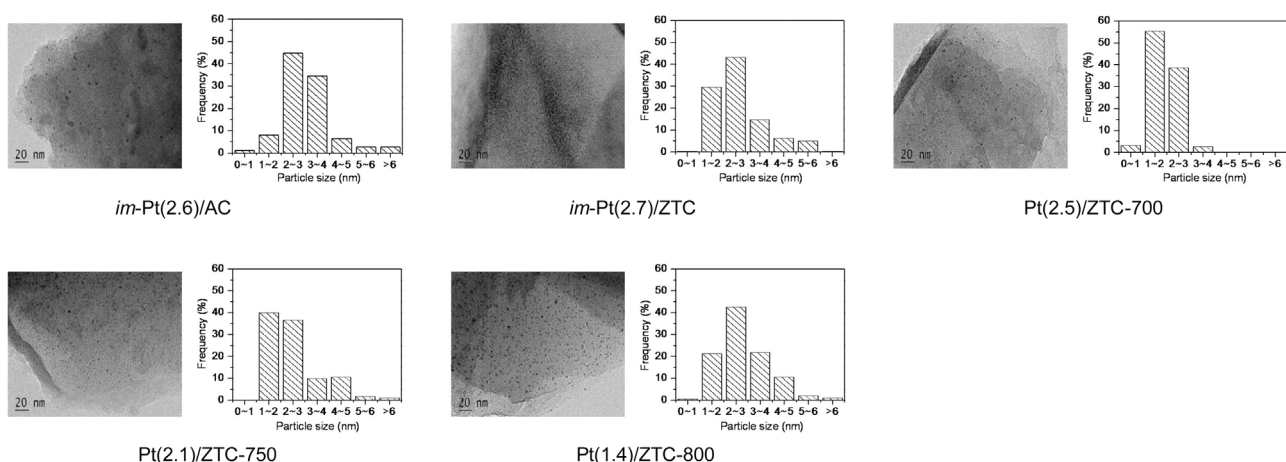


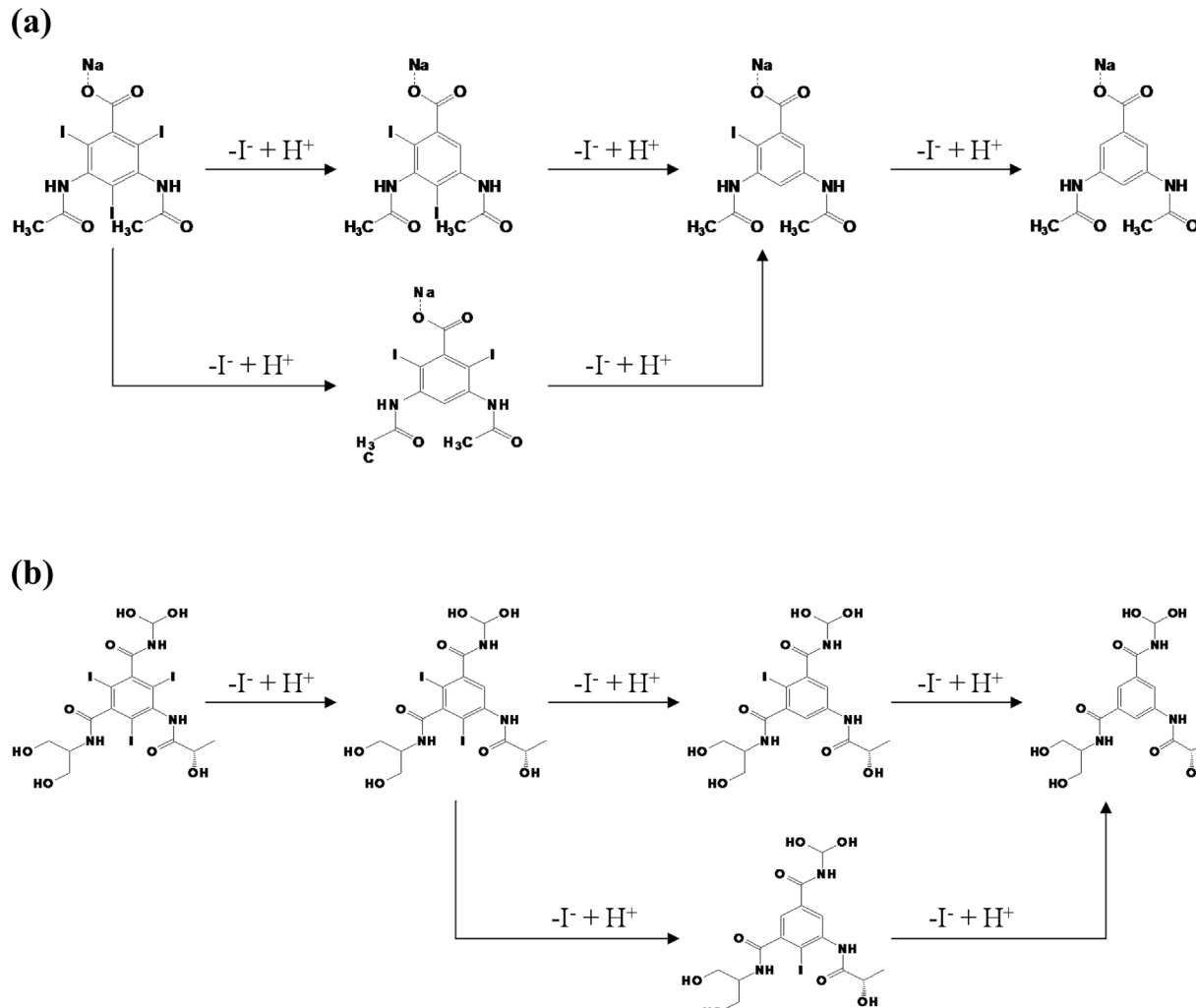
Fig. 3. TEM images and histograms of Pt particle size distributions of supported catalysts.

Table 3
Parameters of XPS spectra of supported Pt catalysts.

	Pt atomic concentration		Binding energy of $\text{Pt}^0 4f_{5/2}$	Binding energy of $\text{Pt}^n + 4f_{5/2}$	$\text{Pt}^n + / \text{Pt}^0$
	Surface ^a (%)	Bulk ^b (%)	(eV)	(eV)	(%)
im-Pt(2.6)/AC	0.29	0.16	71.50	73.42	28
im-Pt(2.7)/ZTC	0.09	0.17	71.51	73.41	41
Pt(2.5)/ZTC-700	0.07	0.16	71.49	73.44	55
Pt(2.1)/ZTC-750	0.05	0.13	71.48	73.38	44
Pt(1.4)/ZTC-800	0.06	0.10	71.47	73.48	20

^a Determined by XPS.

^b Calculated from ICP.



Scheme 1. Catalytic hydrodeiodination pathway of (a) DTZ and (b) IOP.

deiodination pathways, the possible intermediates and products were analyzed using HPLC and LC-TOF-MS operated in the positive mode. Fig. S6 shows HPLC flow spectra from the catalytic hydrodeiodination of DTZ and IOP on Pt(2.5)/ZTC-700. For DTZ hydrodeiodination, one flow peak was observed at retention time of 4.9 min prior to the catalytic reaction, assigned to DTZ. As the reaction proceeded, DTZ concentration gradually decreased, and four new flow peaks concomitantly appeared at 2.0, 2.9, 5.8 and 21.1 min, respectively. The intensities of the peaks at 2.0 and 21.1 min continuously increased, likely from the final products, while the intensities of peaks at 2.9 and 5.8 min first increased and then decreased with the reaction, assigned to the intermediates. The possible intermediates and products were further verified using LC-TOF-MS, and the flow spectra of the samples from DTZ

hydrodeiodination for 30 min are compiled in Fig. S7a. Five peaks with m/z values of 488.9, 631.8, 488.9, 363.0 and 237.1 were obtained, exhibited a mass difference of one or multiples of 126 m/z values, indicative of a sequential deiodination mechanism. Hence, the hydrodehalogenation pathways of DTZ is described in Scheme 1a. Notably, two products with m/z 489 were identified (see Fig. S8b and c), indicating that DTZ deiodination occurred at different substituted sites during the first deiodination step.

Similar to DTZ, sequential deiodination process was also identified on catalytic IOP hydrodeiodination. After reaction for 10 min, the intermediates and products of IOP hydrodeiodination were determined at 2.6, 6.2, 7.9, 9.4, 15.7, and 17.4 min. The intensity of IOP peak gradually decreased with the reaction, while the intensities of the flow

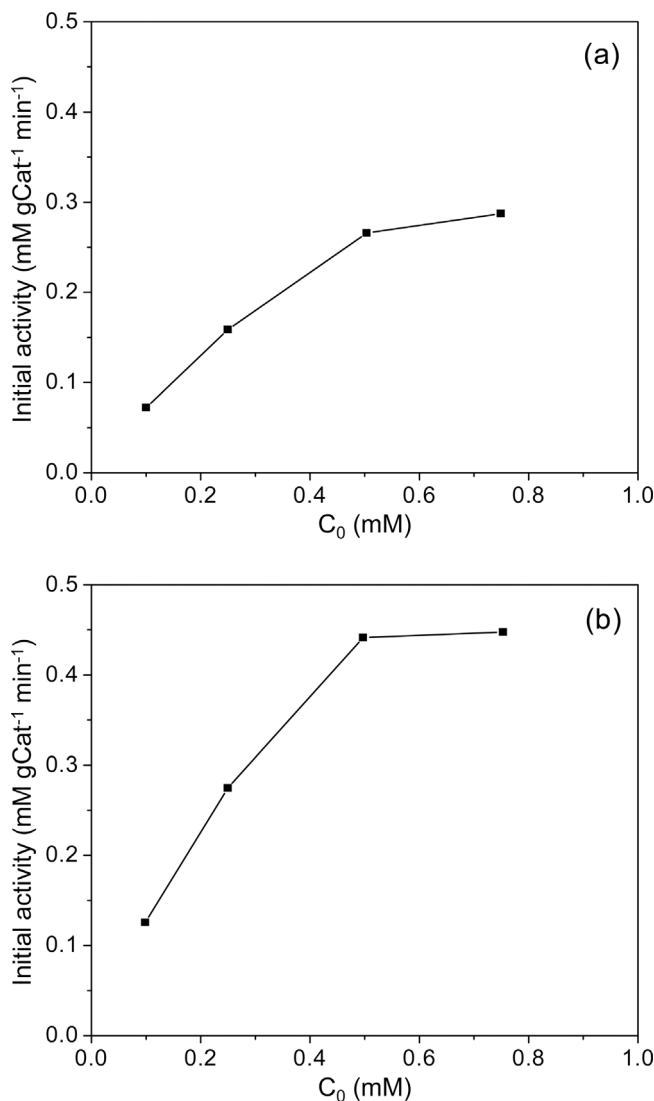


Fig. 4. The initial activity of ICM hydrodeiodination of at varied initial concentrations. (a) DTZ and (b) IOP. Reaction conditions: pH 7; Catalyst: Pt(2.5)/ZTC-700; Catalyst dosage: 0.075 g L^{-1} .

peaks at 2.6 and 17.4 min increased, and the intensities of the flow peaks at 6.2, 9.4 and 15.7 min first increased and then decreased, confirming the presence of multiple intermediates. Fig. S7b shows the LC-TOF-MS spectra of the samples from IOP hydrodeiodination for 10 min. Mass spectra for IOP and its deiodination products were identified with m/z values of 526.1, 777.9, 652.0, 526.1 and 400.2, confirming the sequential hydrodehalogenation pathway. Two peaks assigned to IOP that two iodine were replaced by hydrogen were also determined. In conclusion, the catalytic hydrodeiodination of DTZ and IOP was non-selective and the final products were 3,5-Diacetamido-benzoic acid and *N,N*-Bis(2-hydroxy-1-(hydroxymethyl)ethyl)-5-((2-hydroxy-1-oxopropyl)amino)-1,3-Benzenedicarboxamide, respectively. The reaction pathways of IOP hydrodeiodination are described in Scheme 1b.

Notably, Pt(2.5)/ZTC-700 exhibited different catalytic activities for the hydrodeiodination of IOP and DTZ (See Fig. 5 and Table S1, Supporting information). For example, after reaction for 50 min IOP was completely reduced, while only 82% of DTZ was removed. Accordingly, the initial activity of Pt(2.5)/ZTC-700 for IOP was $0.45 \text{ mM gCat}^{-1} \text{ min}^{-1}$, much higher than that for DTZ ($0.27 \text{ mM gCat}^{-1} \text{ min}^{-1}$). Because the catalytic reaction occurred on catalyst surface, the reaction rate was possibly correlated to ICM

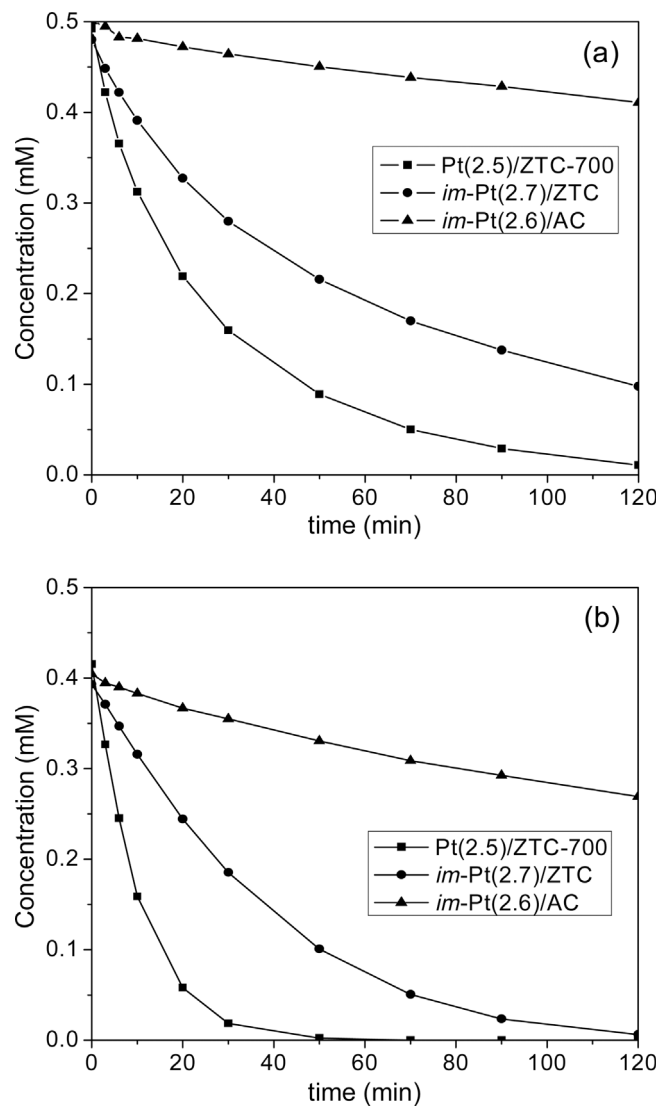


Fig. 5. The catalytic hydrodeiodination of (a) DTZ and (b) IOP on the catalysts with various supports. Reaction conditions: pH 7; Catalyst dosage: 0.075 g L^{-1} ; ICM concentration: 0.5 mM .

adsorption on catalyst surface. Due to the lower solubility of IOP than DTZ [41] in water, stronger IOP adsorption on the catalyst could be expected owing to the stronger hydrophobic interaction between IOP and the catalyst. Additionally, DTZ presented in water in an anionic form, and electrostatic repulsion interaction between DTZ and the catalyst presented because the catalyst was negatively charged at pH 7.0 (see Fig. S4, Supporting information), further suppressing DTZ adsorption on the catalyst. On the contrary, IOP presented in molecular form in water, and IOP adsorption on catalyst surface was favored, giving rise to enhanced IOP hydrodeiodination.

To verify the influence of ICM adsorption on catalytic activity, the catalytic hydrodeiodination of DTZ and IOP with initial concentrations varying from 0.10 to 0.75 mM was conducted on Pt(2.5)/ZTC-700 and the results are presented in Figs. 4 and S10. For DTZ, increasing initial concentration from 0.10 to 0.50 mM resulted in enhanced initial activity from $0.073 \text{ mM gCat}^{-1} \text{ min}^{-1}$ to $0.27 \text{ mM gCat}^{-1} \text{ min}^{-1}$, indicative of positive correlation between adsorbed DTZ concentration and reaction rate. At initial DTZ concentration above 0.50 mM, however, the reaction rate remained almost constant with the increase of DTZ concentration to 0.75 mM, likely due to saturated DTZ adsorption on catalyst within such high DTZ concentration range. Provided that the conversion of adsorbed ICM was a slow reaction (as reflected by the absence of mass

transfer limitations) and adsorption equilibrium was established between aqueous ICM and adsorbed ICM, the dependence of catalytic activity on ICM sorption could thus be clarified by fitting the experimental data to Langmuir-Hinshelwood model [42,43]:

$$r_0 = k\theta_s = \frac{kbC_0}{1 + bC_0} \quad (2)$$

$$\frac{1}{r_0} = \frac{1}{kbC_0} + \frac{1}{k} \quad (3)$$

where r_0 is the initial hydrodeiodination rate at ICM concentration of C_0 , θ_s is the coverage of ICM adsorbed on the catalyst surface, k is the reaction rate constant, and b is the equilibrium constant for ICM adsorption.

The dependence of r_0 on C_0 plotted as $1/C_0$ versus $1/r_0$ is compiled in Fig. S11. Linear relationship with the correlation coefficient (R^2) higher than 0.99 was obtained in the plot of $1/C_0$ versus $1/r_0$, indicating that the catalytic hydrodeiodination of DTZ and IOP on Pt/ZTC followed the Langmuir-Hinshelwood model and the conversion of adsorbed ICM on catalyst surface was the rate controlling step.

The catalytic hydrodeiodination of DTZ and IOP on the catalysts with identical Pt loadings is compared in Fig. 5. Catalytic hydrodeiodination for 120 min led to the removal of DTZ by 98% on Pt(2.5)/ZTC-700, 56% on *im*-Pt(2.7)/ZTC and 14% on *im*-Pt(2.6)/AC. In parallel, IOP was completely converted within 50 min on Pt(2.5)/ZTC-700, and approximately 120 min on *im*-Pt(2.7)/ZTC, while only 40% of IOP was removed within 120 min on *im*-Pt(2.6)/AC, reflecting a decreasing catalytic activity order of Pt(2.5)/ZTC-700 > *im*-Pt(2.7)/ZTC > *im*-Pt(2.6)/AC.

The very different catalytic activities of the catalysts were directly related to their structural properties. As determined by TEM analysis, the average Pt particle sizes were 2.32, 2.98 and 4.01 nm for Pt(2.5)/ZTC-700, *im*-Pt(2.7)/ZTC and *im*-Pt(2.6)/AC, respectively. In principle, Pt particles with smaller particle sizes had larger surface areas and higher contents of exposed Pt active sites, giving rise to higher catalytic activity. Notably, the average Pt particle size of Pt(2.5)/ZTC-700 was slightly smaller than that of *im*-Pt(2.7)/ZTC, whereas the initial activity of Pt(2.5)/ZTC-700 was about 4 times higher for DTZ and 6 times higher for IOP than that of *im*-Pt(2.7)/ZTC, exhibiting unexpectedly higher catalytic activity for catalytic hydrodeiodination. Clearer understanding can be gained by comparing the turnover frequency (TOF) values of active Pt site in the two catalysts. The TOF value was calculated as the initial hydrodeiodination rate of DTZ or IOP per exposed Pt site in the catalyst within initial 10 min, and the number of exposed Pt sites in the catalyst was determined using TEM results. For catalytic DTZ hydrodeiodination, the TOF values of Pt site were calculated to be 0.27 and 0.16 s⁻¹ in Pt(2.5)/ZTC-700 and *im*-Pt(2.7)/ZTC, respectively, indicative of a higher catalytic activity of Pt site in Pt(2.5)/ZTC-700. Previous studies [44] revealed that in liquid phase catalytic hydrodehalogenation reactions activation of H₂ and carbon-halogen (C-X) band were two crucial reaction steps for the effective clearance of C-X bands [45,46], in which metallic and cationic noble metal species served as the respective active sites. Notably, XPS analysis indicated that Pt⁴⁺ and Pt⁰ coexisted in the catalysts. Additionally, the content of Pt⁴⁺ in Pt(2.5)/ZTC-700 was 37%, higher than that in *im*-Pt(2.7)/ZTC (28%). Considering the much higher TOF value of Pt site in Pt(2.5)/ZTC-700, it could also be concluded that the activation of C-X bonds played a more important role in the catalytic hydrodeiodination as compared with H₂ activation. In parallel, the TOF of Pt site in Pt(2.5)/ZTC-700 and *im*-Pt(2.7)/ZTC were 0.47 and 0.30 s⁻¹ for the catalytic hydrodeiodination for IOP, also confirming the more importance role of C-X activation on the catalyst. Similar results were also observed previously [47]. It was noteworthy that TOF values of the catalysts were much higher than those previously reported in the hydrodechlorination reactions [15,48], also highlighting the advantages of the *in-situ* CVD method.

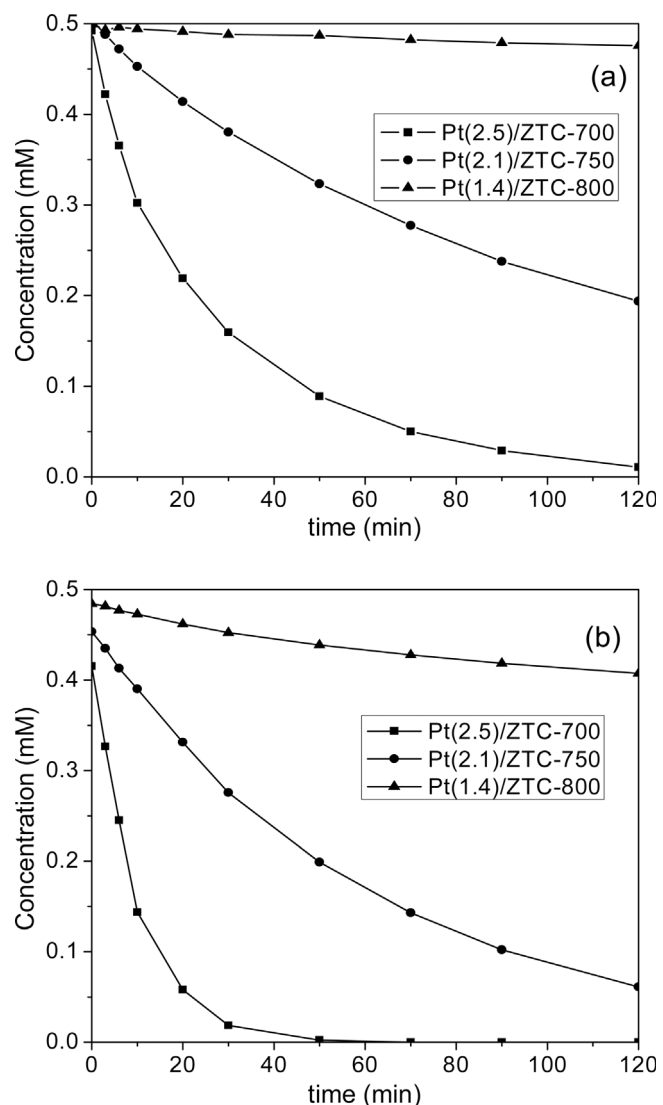


Fig. 6. The catalytic hydrodeiodination of (a) DTZ and (b) IOP on the catalysts prepared at varied CVD temperatures. Reaction conditions: pH 7. Catalyst dosage: 0.075 g l⁻¹; ICM concentration: 0.5 mM.

The activities of the catalysts were strongly dependent on CVD temperature, and the catalytic hydrodeiodination of DTZ and IOP on the catalysts prepared at varied CVD temperatures is shown in Fig. 6. For both DTZ and IOP, the catalyst prepared at lower CVD temperature exhibited a higher catalytic activity. Although identical precursor Pt/Y zeolite was used, CVD at higher temperature resulted in a lower Pt loading due to more facile carbon deposition on zeolite. Hence, a lower catalytic activity could be expected on the catalyst prepared at higher CVD temperature due to the low Pt content. Notably, the initial catalytic activity of Pt(2.5)/ZTC-700 for DTZ hydrodeiodination was 0.27 mM gCat⁻¹ min⁻¹, which was 4 times as high as that of Pt(2.1)/ZTC-750 and 38 times as high as that of Pt(1.4)/ZTC-800. Similarly, the catalytic activity of Pt(2.5)/ZTC-700 for IOP hydrodeiodination was 4 times as high as that of Pt(2.1)/ZTC-750 and 12 times as high as that of Pt(1.4)/ZTC-800. Considering that Pt loading in Pt(2.5)/ZTC-700 was only slightly higher than Pt(2.1)/ZTC-750 and about two times as high as that of Pt(1.4)/ZTC-800, the unexpectedly high catalytic activity of Pt(2.5)/ZTC-700 for catalytic hydrodeiodination of DTZ and IOP indicated that Pt loading was not the only factor controlling the catalytic activity. Again, the TOF values were calculated to be 0.27, 0.085 and 0.021 s⁻¹ for DTZ hydrodeiodination on Pt(2.5)/ZTC-700, Pt(2.1)/ZTC-750, and Pt(1.4)/ZTC-800, respectively, indicating that the

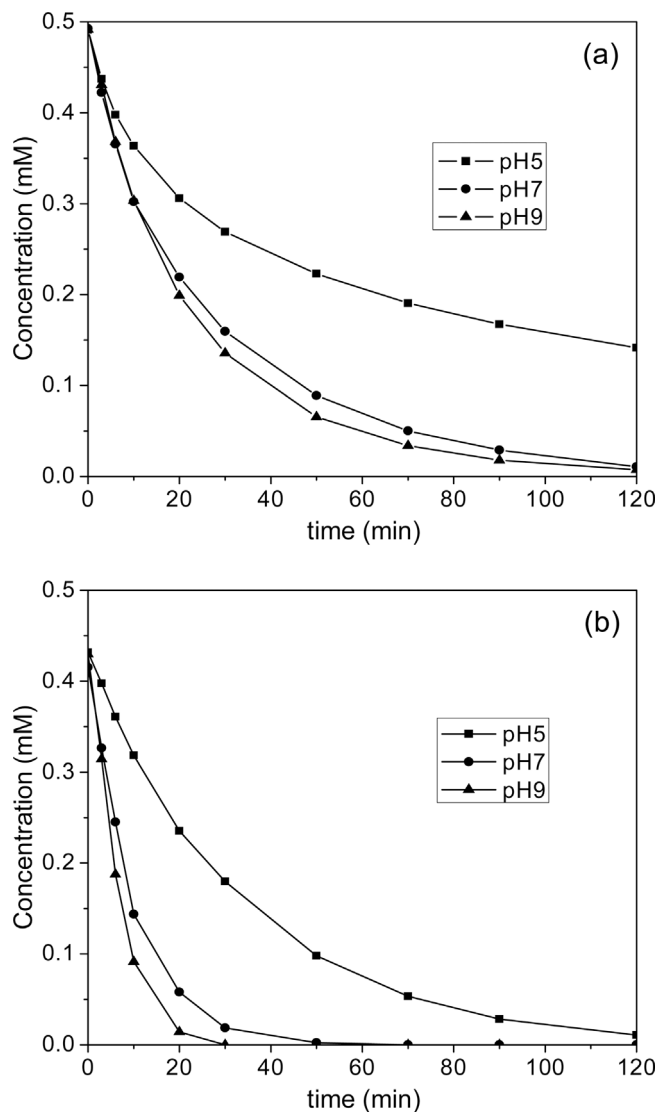


Fig. 7. Influence of pH on the hydrodeiodination of ICM on Pt(2.5)/ZTC-700. (a) DTZ; (b) IOP. Reaction conditions: Catalyst dosage: 0.075 g l^{-1} , ICM concentration: 0.5 mM .

catalytic activity of Pt site was negatively correlated to CVD temperature. Similar results were also observed for the catalytic IOP hydrodeiodination on the three catalysts. XPS analysis revealed that $\text{Pt}^{n+}/\text{Pt}^0$ ratios decreased with CVD temperature in the catalysts, accounting for the decreased catalytic activity of Pt site with CVD temperature. Furthermore, the negative relationship between the activity of Pt site and CVD temperature again confirmed the crucial role of activation of C-I bond for the catalytic hydrodeiodination of DTZ and IOP.

The influence of pH on the catalytic activity of Pt(2.5)/ZTC-700 for ICM hydrodeiodination was investigated and the results are compiled in Fig. 7. For DTZ, the initial reaction rates were determined to be 0.18, 0.27, and $0.27 \text{ mM gCat}^{-1} \text{ min}^{-1}$ at pH of 5, 7, and 9, respectively, reflecting an enhanced catalytic hydrodeiodination with the increase of pH. Similar trend was also observed for the catalytic IOP hydrodeiodination on Pt(2.5)/ZTC-700. Previous studies [48,49] also observed pH dependent catalytic activity in liquid catalytic hydrogenation. As demonstrated above, the catalytic hydrodeiodination rate was strongly dependent on ICM adsorption. Thus, variation of the concentration of adsorbed ICM with pH on the catalysts may impact the catalytic hydrodeiodination. For DTZ, increasing pH evoked electrostatic repulsive interaction between DTZ and catalyst surface because DTZ presented in an anionic form under the experimental conditions, likely leading to decreased catalytic activity due to suppressed DTZ

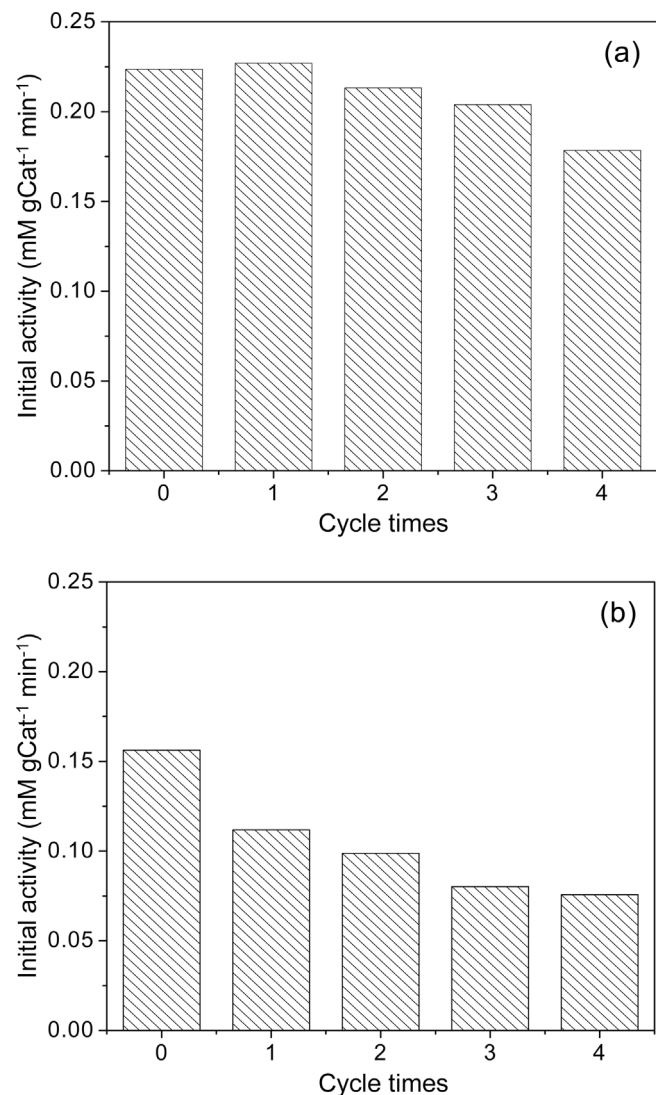


Fig. 8. The reusability of (a) Pt(2.5)/ZTC-700 and (b) im-Pt(2.7)/ZTC for the hydrodeiodination of DTZ. Reaction conditions: pH 7; Catalyst dosage: 0.075 g l^{-1} for Pt(2.5)/ZTC-700 and 0.1 g l^{-1} for im-Pt(2.7)/ZTC, DTZ concentration: 0.5 mM .

adsorption. As for IOP, changing pH only resulted in a minor influence on IOP adsorption because IOP existed in water in a molecular form, and negligible pH dependence effect could be expected, which was contrary to the experimental results. Hence, ICM adsorption did not play a predominant role in the dependence of catalytic ICM conversion on pH. Notably, Ma et al. [50] concluded that adsorption of I^- on the surface of the catalysts from catalytic hydrodeiodination blocked active sites, and thus markedly suppressed the catalytic activity. In parallel, Dong et al. [51] found that catalytic hydrodechlorination of 4-chlorophenol at high pH effectively inhibited the adsorption of Cl^- on noble metal surface, thus enhancing the catalytic activity. Accordingly, the increased catalytic hydrodeiodination activity of Pt(2.5)/ZTC-700 with pH could be attributed to the effective removal of I^- from catalyst surface.

To examine the stability of Pt(2.5)/ZTC-700, the catalytic hydrodeiodination of DTZ on Pt(2.5)/ZTC-700 and im-Pt(2.7)/ZTC was compared, and the results are presented in Fig. 8. For Pt(2.5)/ZTC-700, the initial activity decreased from 0.22 to $0.18 \text{ mM gCat}^{-1} \text{ min}^{-1}$ after 4 catalyst reuse cycles, reflecting a slow catalyst deactivation. In contrast, 4 catalyst reuse cycles led to a marked decrease of the initial catalytic activity of im-Pt(2.7)/ZTC from 0.16 to $0.08 \text{ mM gCat}^{-1} \text{ min}^{-1}$. Previous studies showed that in batch reaction

noble metal catalysts supported on carbon supports displayed marked catalyst deactivation, predominantly due to noble metal loss [52]. Additionally, large-sized metal particle were more susceptible to loss during the reaction process. For Pt(2.5)/ZTC-700, the majority of noble metal particles were confined in the pores of ZTC or embedded beneath ordered microporous carbon, exhibiting strong resistance to Pt particle loss. Thus, the slow catalyst deactivation was probably due to the loss of some noble metal particles located on the external surface of the catalyst. As for *im*-Pt(2.7)/ZTC, however, the majority of Pt particles were located on the external surface of carbon support, as reflected by TEM and XPS analysis. Additionally, the average particle size of Pt particles was larger than that of Pt(2.5)/ZTC-700. Therefore, more marked Pt metal loss could be expected on *im*-Pt(2.7)/ZTC, giving rise to more serious catalyst deactivation than that of Pt(2.5)/ZTC-700. Accordingly, the residual Pt contents in the catalysts were determined by ICP after four catalyst reuse cycles for catalytic DTZ hydrodeiodination and were found to be 2.2 wt.% and 1.5 wt.% in Pt(2.5)/ZTC-700 and *im*-Pt(2.7)/ZTC, respectively. The much more remarkable Pt loss on *im*-Pt(2.7)/ZTC than on Pt(2.5)/ZTC-700 was in good agreement with the activity data.

4. Conclusions

In the present study, Pt catalysts supported on ordered microporous carbon were prepared by an *in-situ* CVD method using Pt exchanged Y zeolite as the template, and the catalytic hydrodeiodination of two ICM (i.e., diatrizoate and iopamidol) was conducted. Despite of preparation at a very high CVD temperature, Pt(2.5)/ZTC-700 displays a higher Pt dispersion and more homogeneous Pt particle distribution than *im*-Pt(2.7)/ZTC, due to confinement and embedment effects. Additionally, cationic Pt species are identified in the supported catalysts, and a higher ratio of $\text{Pt}^{\text{n}+}/\text{Pt}^0$ presents on Pt(2.5)/ZTC-700 than *im*-Pt(2.7)/ZTC, resulting from a stronger metal-support interaction. For catalytic hydrodeiodination of both DTZ and IOP, Pt(2.5)/ZTC-700 exhibits much higher catalytic activities than *im*-Pt(2.7)/ZTC. As for catalytic hydrodeiodination of DTZ and IOP, more effective removal of IOP is achieved, attributed to its stronger adsorption than DTZ on Pt(2.5)/ZTC-700. Accordingly, the catalytic hydrodeiodination of DTZ and IOP follows the Langmuir-Hinshelwood model, indicative of an adsorption controlling reaction mechanism. Furthermore, the TOF value of Pt/ZTC decreases with CVD temperature due to decreased $\text{Pt}^{\text{n}+}/\text{Pt}^0$ ratio in the catalyst. High pH effectively suppresses iodine adsorption on catalyst surface, thus facilitating catalytic hydrodeiodination of DTZ and IOP. As for catalyst reuse, Pt(2.5)/ZTC-700 exhibits a higher stability than *im*-Pt(2.7)/ZTC, resulting from effective confinement and embedment effects.

Acknowledgements

The financial support from the National Natural Science Foundation of China (No. 21237002, 21577056 and 21507056), and the Natural Science Foundation of Jiangsu Province (BK20150568) is gratefully acknowledged.

Appendix A. Supplementary data

Supplementary data associated with this article can be found, in the online version, at <http://dx.doi.org/10.1016/j.apcatb.2017.10.006>.

References

- [1] E. Borowska, E. Felis, S. Żabczyński, Water Air Soil Pollut. 226 (2015) 151–163.
- [2] B. De Gusseme, T. Hennebel, L. Vanhaecke, M. Soetaert, J. Desloover, K. Wille, K. Verbeken, W. Verstraete, N. Boon, Environ. Sci. Technol. 45 (2011) 5737–5745.
- [3] A. Putschew, S. Schittko, M. Jekel, J. Chromatogr. A 930 (2001) 127–134.
- [4] A. Putschew, S. Wischnack, M. Jekel, Sci. Total Environ. 255 (2000) 129–134.
- [5] A.S. Mestre, M. Machuqueiro, M. Silva, R. Freire, I.M. Fonseca, M. Soledade, C.S. Santos, M.J. Calhorda, A.P. Carvalho, Carbon 77 (2014) 607–615.
- [6] T. Matsushita, N. Kobayashi, M. Hashizuka, H. Sakuma, T. Kondo, Y. Matsui, N. Shirasaki, Chemosphere 135 (2015) 101–107.
- [7] S.P.D. Barceló, Anal. Bioanal. Chem. 387 (2007) 1235–1246.
- [8] S.E. Duirk, C. Lindell, C.C. Cornelison, J. Kormos, T.A. Ternes, M. Attene-Ramos, J. Osiol, E.D. Wagner, M.J. Plewa, S.D. Richardson, Environ. Sci. Technol. 45 (2011) 6845–6854.
- [9] S.U. Yoon, B. Mahanty, C.G. Kim, Desalin. Water Treat. 57 (2015) 7789–7800.
- [10] A.S. Mestre, R.A. Pires, I. Aroso, E.M. Fernandes, M.L. Pinto, R.L. Reis, M.A. Andrade, J. Pires, S.P. Silva, A.P. Carvalho, J. Chem. Eng. 253 (2014) 408–417.
- [11] S.P. Azerrad, S.G. Reznik, L.H. Grossman, C.G. Dosoretz, Water Res. 62 (2014) 107–116.
- [12] I. Velo-Gala, J.J. López-Peña, M.S. Polo, J.R. Utrilla, J. Chem. Eng. 241 (2014) 504–512.
- [13] D. Shuai, B.P. Chaplin, J.R. Shapley, N.P. Menendez, D.C. McCalman, W.F. Schneider, C.J. Werth, Environ. Sci. Technol. 44 (2010) 1773–1779.
- [14] I. Forrez, M. Carballa, G. Fink, A. Wick, T. Hennebel, L. Vanhaecke, T. Ternes, N. Boon, W. Verstraete, Water Res. 45 (2011) 1763–1773.
- [15] L.E. Kinitt, J.R. Shapley, T.J. Strathmann, Environ. Sci. Technol. 42 (2008) 577–583.
- [16] J.A. Baeza, L. Calvo, M.A. Gilarranz, J.J. Rodriguez, J. Chem. Eng. 240 (2014) 271–280.
- [17] M.A. Keane, J. Chem. Technol. Biotechnol. 80 (2005) 1211–1222.
- [18] L.M. Gomez-Sainero, A. Cortés, X.L. Seiane, A. Arcoya, Ind. Eng. Chem. Res. 39 (2000) 2849–2854.
- [19] E. Diaz, A.F. Mohedano, J.A. Casas, J.J. Rodriguez, Appl. Catal. B Environ. 181 (2016) 429–435.
- [20] S. Ordóñez, B.P. Vivas, F.V. Díez, Appl. Catal. B Environ. 95 (2010) 288–296.
- [21] C.B. Molina, A.H. Pizarro, J.A. Casas, J.J. Rodriguez, Appl. Catal. B Environ. 148–149 (2014) 330–338.
- [22] C.E. Chan-Thaw, A. Villa, P. Katekomol, D.S. Su, A. Thomas, L. Prati, Nano Lett. 10 (2010) 537–541.
- [23] G. Yuan, M.A. Keane, Appl. Catal. B Environ. 52 (2004) 301–314.
- [24] C.H. Choi, M. Kin, H.C. Kwon, S.J. Cho, S. Yun, H.T. Kim, K.J.J. Mayrhofer, H. Kim, M. Chio, Nat. Commun. 7 (2016) 10922.
- [25] Y. Shao, Z. Xu, H. Wan, Y. Wan, H. Chen, S. Zheng, D. Zhu, Catal. Commun. 12 (2011) 1405–1409.
- [26] Z. Guo, C. Xiao, R.V. Maligal-Ganesh, L. Zhou, T.W. Goh, X. Li, D. Tesfagaber, A. Thiel, W. Huang, ACS Catal. 4 (2014) 1340–1348.
- [27] J. Mondal, S.K. Kundu, W.K. Hung Ng, R. Singuru, P. Borach, H. Hirao, Y. Zhao, A. Bhaumik, J. Chem. Eur. 21 (2015) 19016–19027.
- [28] H.N. Yang, S.H. Park, D.C. Lee, S.C. Yi, W.J. Kim, Micropor. Mesopor. Mater. 172 (2013) 161–166.
- [29] N. Alam, R. Mokaya, Micropor. Mesopor. Mater. 142 (2011) 716–724.
- [30] E.N. Coker, W.A. Steen, J.T. Miller, A.J. Kropf, J.E. Miller, Micropor. Mesopor. Mater. 101 (2007) 440–444.
- [31] E.N. Coker, W.A. Steen, J.E. Miller, Micropor. Mesopor. Mater. 104 (2007) 236–247.
- [32] T.J. Lim, S.Y. Lee, Y.J. Yoo, S.J. Park, Bull. Korean Chem. Soc. 35 (2014) 3576–3582.
- [33] N. Alam, R. Mokaya, Energy Environ. Sci. 3 (2010) 1773–1781.
- [34] N.P. Stadie, S. Wang, K.V. Kravchyk, M.V. Kovalenko, ACS Nano 11 (2017) 1911–1919.
- [35] J. Zhou, L. Wen, Z. Zhang, X. Wu, W. Xing, S. Zhuo, Electrochim. Acta 89 (2013) 763–770.
- [36] T.J. Lim, S.Y. Lee, Y.J. Yoo, S.J. Park, B. Korean Chem. Soc. 35 (2014) 3576–3582.
- [37] M. Martin-Martinez, L.M. Gómez-Sainero, J. Bedia, A.A. Bastante, J.J. Rodriguez, Appl. Catal. B Environ. 184 (2016) 55–63.
- [38] M. Martin-Martinez, A. Álvarez-Montero, L.M. Gómez-Sainero, R.T. Baker, J. Palomar, S. Omar, S. Esenc, J.J. Rodriguez, Appl. Catal. B Environ. 162 (2015) 532–543.
- [39] X. Ning, Y. Li, B. Dong, H. Wang, H. Yu, F. Peng, Y. Yang, J. Catal. 348 (2017) 100–109.
- [40] A. Arevalo-Bastante, M.A. Álvarez-Montero, J. Bedia, L.M. Gómez-Sainero, J.J. Rodriguez, Appl. Catal. B Environ. 179 (2015) 551–557.
- [41] A. Mendoza, B. Zonja, N. Mastrianni, N. Negreira, M. López de Alda, S. Pérez, D. Barceló, A. Gil, Y. Valcárcel, Environ. Int. 86 (2016) 107–118.
- [42] A. Pintar, J. Batista, J. Levec, T. Kajiuchi, Appl. Catal. B: Environ. 11 (1996) 81–98.
- [43] Z.M. Pedro, J.A. Casas, L.M. Gómez-Sainero, J.J. Rodriguez, Appl. Catal. B: Environ. 98 (2010) 79–85.
- [44] M. Bonarowska, Z. Kaszku, L. Kepiński, Z. Karpinski, Applied catalysis appl., Catal. B Environ. 99 (2010) 248–256.
- [45] L.M. Gómez-Sainero, X.L. Seoane, J.L.G. Fierro, A. Arcoya, J. Catal. 209 (2002) 279–288.
- [46] J. Andersin, P. Parkkinen, K. Honkala, J. Catal. 290 (2012) 118–125.
- [47] K. Wu, M. Zheng, Y. Han, Z. Xu, S. Zheng, Appl. Surf. Sci. 376 (2016) 113–120.
- [48] G. Yuan, M.A. Keane, J. Catal. 225 (2004) 510–522.
- [49] M.A. Aramendia, R. Burch, I.M. García, A. Marinas, J.M. Marinas, B.W.L. Southward, F.J. Urbano, Appl. Catal. B Environ. 31 (2001) 163–171.
- [50] X. Ma, S. Liu, Y. Liu, G. Gu, C. Xia, Sci. Rep. 6 (2016) 484–995.
- [51] Z. Dong, X. Le, C. Dong, W. Zhang, X. Li, J. Ma, Appl. Catal. B Environ. 162 (2015) 372–380.
- [52] W. Sun, Q. Li, S. Gao, J.K. Shang, J. Mater. Chem. A 1 (2013) 9215–9224.